Direct kinetochore–spindle pole connections are not required for chromosome segregation

Vitali Sikirzhytski,[1] Valentin Magidson,[1] Jonathan B. Steinman,[2] Jie He,[1] Maël Le Berre,[3] Irina Tikhonenko,[1] Jeffrey G. Ault,[1] Bruce F. McEwen,[1] James K. Chen,[4] Haixin Sui,[1] Matthieu Piel,[3] Tarun M. Kapoor,[2] and Alexey Khodjakov[1,5]

[1]Wadsworth Center, New York State Department of Health, Albany, NY 12201
[2]Rockefeller University, New York, NY 10021
[3]Institut Curie, 75248 Paris, France
[4]Stanford School of Medicine, Stanford, CA 94305
[5]Rensselaer Polytechnic Institute, Troy, NY 12180

Segregation of genetic material occurs when chromosomes move to opposite spindle poles during mitosis. This movement depends on K-fibers, specialized microtubule (MT) bundles attached to the chromosomes' kinetochores. A long-standing assumption is that continuous K-fibers connect every kinetochore to a spindle pole and the force for chromosome movement is produced at the kinetochore and coupled with MT depolymerization. However, we found that chromosomes still maintained their position at the spindle equator during metaphase and segregated properly during anaphase when one of their K-fibers was severed near the kinetochore with a laser microbeam. We also found that, in normal fully assembled spindles, K-fibers of some chromosomes did not extend to the spindle pole. These K-fibers connected to adjacent K-fibers and/or nonkinetochore MTs. Poleward movement of chromosomes with short K-fibers was uncoupled from MT depolymerization at the kinetochore. Instead, these chromosomes moved by dynein-mediated transport of the entire K-fiber/kinetochore assembly. Thus, at least two distinct parallel mechanisms drive chromosome segregation in mammalian cells.

Introduction

Proper chromosome segregation during cell division requires a complex series of movements. During the first half of mitosis (prometaphase–metaphase), chromosomes congress into a tight group (termed metaphase plate) near the equator of mitotic apparatus (spindle). At later stages (anaphase–telophase), each chromosome splits into two chromatids and the chromatids move toward the opposite spindle poles.

Chromosome movements occur in a crowded space and are driven by strong forces (Nicklas, 1983; Ferraro-Gideon et al., 2013). Connections between chromosomes and spindle poles must withstand these forces or else some chromosomes will be left behind, resulting in aneuploid cells. The question of how each chromosome maintains a continuous strong connection to the spindle pole is therefore paramount for understanding the mechanisms that govern faithful chromosome segregation.

In higher eukaryotes, chromosomes attach to bundles of ∼20 microtubules (MTs; termed K-fibers) via discrete macromolecular assemblies termed kinetochores (Walczak et al., 2010). EM demonstrates that K-fibers of many chromosomes extend from the kinetochore to the spindle pole and at least some MTs within a K-fiber are continuous (Rieder, 1981; Witt et al., 1981; Church and Lin, 1982; Nicklas et al., 1982; McDonald et al., 1992). These studies inspired the currently dominant view that in fully assembled spindles every chromosome is directly connected to the poles. However, this notion should not be considered proven. Because of technical limitations, the complete architecture of the mammalian spindle has not been reconstructed at a sufficiently high resolution and therefore whether all chromosomes connect directly to the poles remains unknown.

Here we provide evidence that some K-fibers in mammalian cells do not connect directly to the pole. Instead, the distal (with respect to the kinetochore) ends of these short K-fibers interact dynamically with the K-fibers of adjacent chromosomes

V. Sikirzhytski and V. Magidson contributed equally to this paper.
Correspondence to A. Khodjakov: alexey.khodjakov@health.ny.gov
Abbreviations used in this paper: LM, light microscopy; MT, microtubule.

The Rockefeller University Press $30.00
J. Cell Biol. Vol. 206 No. 2 231–243
www.jcb.org/cgi/doi/10.1083/jcb.201401090

and/or other MTs within the spindle. These interactions, mediated by the minus end–directed MT motor dynein, are sufficient to move chromosomes poleward during anaphase. Thus, chromosome segregation is effected by at least two distinctly different mechanisms that act in parallel during mitosis in mammalian cells.

Results

Chromosomes that lack a direct K-fiber connection to the spindle pole remain bioriented

We used a highly focused laser microbeam (Magidson et al., 2007) to sever individual K-fibers on fully congressed chromosomes in PtK_2 (marsupial) and RPE-1 (human, nontransformed) cells with fluorescently labeled MTs. The beam was aimed at the fiber ∼1 µm in front of the kinetochore (Fig. 1 A). Successful severing of the fiber was evident from rapid depolymerization of the K-fiber fragment attached to the spindle pole as well as from changes in the orientation of the short MT stub that remained attached to the kinetochore (Fig. 1 A′ and Video 1).

The length of the K-fiber stub increased monotonically at ∼1.0 µm/min. This elongation was consistent with the notion that the minus ends of severed MTs are stable whereas the plus ends continue to incorporate new MT subunits at the kinetochore (Maiato et al., 2004, 2005). Indeed, the K-fiber elongation rate matched closely to the rate of poleward MT flux in the same cell line (1.1 ± 0.4 µm/min; Fig. S1 A). Because of the continuous elongation of the stub, the minus ends of severed K-fibers should reach the spindle pole, restoring a direct connection between the kinetochore and the spindle pole in 5–7 min (Maiato et al., 2004).

Kymogram analysis demonstrated that the distance between sister kinetochores decreased instantly after the laser burst. This sudden loss of centromere tension implied that the poleward force that acted along the K-fiber ceased when the K-fiber was severed. However, centromere stretch was usually restored in <30 s, long before the K-fiber stub could regrow to reach the spindle pole (Fig. 1 A″). Instead, restoration of centromere tension occurred when the stub appeared to contact an adjacent MT bundle (Fig. 1 A′ and Video 1). This contact occurred on average 5.3 ± 1.0 s after the laser burst (the full compilation of the numeric data for laser microsurgery experiment is presented in Table S1) and it resulted in a rapid jump of the entire stub poleward. The poleward velocity during the jump was significantly higher than the velocity of oscillating bioriented chromosomes (4.7 ± 0.7 vs. 2.4 ± 0.7 µm/min, P = 0.014).

Consistent with the observed rapid restoration of poleward forces, in PtK_2 cells, 95% (57/60) of chromosomes with severed K-fibers maintained their position near the spindle equator despite the lack of a direct connection to one of the spindle poles. In the remaining 5% (3/60), the stub reoriented toward the opposite spindle pole (Fig. S1 C and Video 2). Reorientation occurred via a gliding motion of the stub's minus end alongside MT bundles connected to the opposite spindle pole (Fig. S1 C and Video 2). As a result of K-stub reorientation, the chromosome became syntelic (attached to the same pole with both kinetochores) and moved to the vicinity of the pole (Fig. S1 C and Video 2).

Because of the low intensity of the excitation light (necessary to avoid photodamage) as well as the relatively short image acquisition times (necessary for capturing dynamic processes), a large number of spindle MTs escape detection in the live-cell recordings (Fig.1, compare B and B″). Therefore, we used correlative light microscopy (LM)/EM and fixed-cell immunofluorescence to detail the character of interactions between the K-fiber stubs and the spindle. Cells with severed K-fibers were fixed on the microscope stage as soon as poleward movement of the severed K-fiber was detected (30–40 s after the laser burst; Video 3).

A depression in fluorescence intensity of GFP–α-tubulin was reproducibly observed between the ends of the stubs and the adjacent bundles in higher signal/noise fluorescence datasets obtained from fixed cells (Fig. 1 B″; $n = 30$). This depression suggested that the minus ends of most MTs within the severed fiber were not directly attached to other MTs. An increase in fluorescence intensity is expected when two objects are separated by less than the diffraction spot (∼200 nm in images).

Serial-section EM reconstructions of four severed fibers confirmed that the majority of the severed MT minus ends were free. Only some resided in the immediate proximity of other spindle MTs. Similar proximity between MTs of the stubs and adjacent spindle MTs was observed at multiple points along the entire length of the stub (Fig. 1, C and D). However, whether direct interaction between MTs in fact occurred at these proximity points could not be determined in serial-section reconstructions of chemically fixed cells.

Immunofluorescence analyses suggested that interaction with just a single spindle MT at the tip of the stub may be sufficient to fully stretch the centromere (Fig. S1 D). It also revealed that the ends of severed fibers were decorated with NuMA (Fig. S1 D), a protein essential for the formation and maintenance of properly focused spindle poles (Merdes et al., 1996; Dionne et al., 1999; Radulescu and Cleveland, 2010). NuMA was recruited to the severed fibers in <30 s after the cut.

Chromosomes lacking direct connection to the pole can segregate during anaphase

To determine whether chromosomes that lack direct connections with spindle poles can segregate, we severed individual K-fibers shortly after the onset of anaphase (Fig. 2). Kymograms demonstrated that chromosomes with severed K-fibers stopped abruptly. However, poleward movement soon resumed and the entire stub with the attached chromosome was transported poleward (Figs. 2 A and S2 A). The transport initiated when the stub appeared to contact neighboring MTs (Fig. 2 A′ and Video 4). In some instances, a single rapid gliding motion delivered the chromosome to the pole (Fig. S2 A′ and Video 5). However, most chromosomes displayed a series of rapid (up to 10 µm/min) yet brief (<10 s) jumps that were intermittent with stationary periods (Fig. 2 A″). In spite of the unusual patterns of movement, all chromosomes with K-fibers severed during anaphase ($n = 14$) reached the spindle poles and were incorporated into the daughter nuclei (Fig. 2 B).

During anaphase in vertebrate cells, both the plus and minus ends of K-fiber MTs are expected to depolymerize steadily (Fig. S1 B). However, the length of K-fiber stubs created

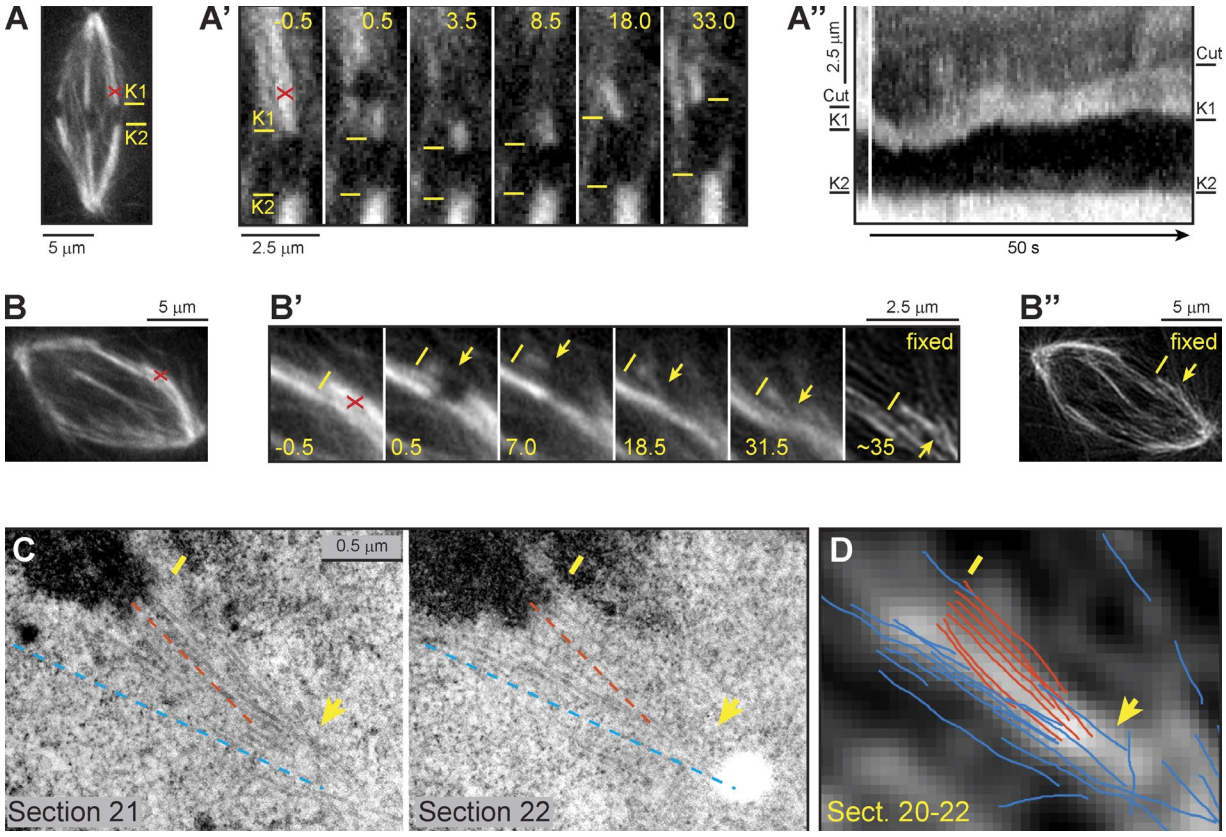

Figure 1. **Continuous K-fiber connection to the spindle pole is not required for chromosome biorientation.** (A–A″) Behavior of a laser-severed K-fiber during metaphase in a PtK_2 cell. (A) Overview of the cell. (A′) Selected frames from time-lapse recording. Laser pulses aimed ∼1 µm in front of kinetochore (X) break the fiber into two fragments. The fragment attached to the spindle pole rapidly depolymerizes. In contrast, the stub attached to the kinetochore (yellow lines) changes orientation, appears to contact neighboring MTs, and subsequently moves slightly toward the spindle pole. (A″) Kymogram generated from the recording used for A′. Notice a sudden decrease of the distance between sister kinetochores followed by a rapid restoration of centromere stretching. Also notice a gradual increase in the length of K-fiber stub during the course of the experiment. K1 and K2, estimated positions of sister kinetochores; Cut, position of laser cut and minus end of the K-fiber stub. (B–D) Laser-severed K-fibers form contacts with adjacent MT bundles. (B) Overview of the cell before operation. (B′) Selected frames from time-lapse recording (similar to A). The cell was fixed soon after the stub initiated poleward movement. (B″) Selected focal plane from deconvolved 3D GFP fluorescence volume recorded after fixation. Notice numerous spindle MTs that are not detected in the live-cell recording. (C) Two consecutive 150-nm EM sections containing the kinetochore with severed K-fiber. Notice that the stub (orange dashed lines) crosses another MT bundle (blue dashed lines). (D) Tracing of MTs in three consecutive EM sections superimposed on the corresponding fluorescence planes. Yellow lines mark positions of the kinetochore and arrows point to the minus end of the stub. Time stamp in seconds from the time of laser irradiation.

shortly after the onset of anaphase remained constant (Fig. 2 A″). This observation indicated that the loss of direct connection to the spindle pole somehow stabilized the MTs of the stub. To test this possibility, we created fiduciary marks on K-fibers by photobleaching short segments of MTs ∼1 µm in front of the kinetochore with a continuous-wave 488-nm laser (Fig. 2 B). To achieve the image clarity necessary for tracking severed K-fibers with bleached segments, we restricted the rounding of mitotic cells by placing a hard ceiling above the coverslip with growing cells (Le Berre et al., 2012). Chromosome movements in flattened cells have been shown to be normal (Lancaster et al., 2013). Behavior of chromosomes with severed fluorescently labeled K-fibers was similar to that observed in rounded cells (Fig. S2 B, Video 6, and Table S1). In both PtK_2 and RPE1 cells, the K-fiber stubs exhibited poleward jumps at a mean poleward velocity >4.5 µm/min, whereas bioriented chromosomes with intact K-fibers moved at 2.2 µm/min (Table S1). The only difference observed was that the mean duration of the period between fiber severing and the initiation of the fast poleward movement was longer in flattened than in rounded ones (11.3 ± 1.5 vs. 5.3 ± 1.0 s, P = 0.003 in PtK_2, and 13.8 ± 1.7 vs. 5.2 ± 0.6 s, P = 0.008 in RPE1). Presumably, this delay was caused by a lower density of MTs within the flattened spindle that decreased the probability of contacts between the K-fiber stub and the neighboring MTs.

Kinetochores are expected to move poleward faster than the bleached segments if the plus ends depolymerize at the kinetochore (i.e., Pacman activity; Gorbsky et al., 1987; Nicklas, 1989; Inoué and Salmon, 1995). Indeed, we observed this behavior for kinetochores directly attached to the pole via continuous K-fibers (Fig. 2 D and Video 7; $n = 9$). In contrast, the distance between kinetochores and bleached segments remained constant during the rapid poleward transport of K-fibers stubs (Fig. 2 D′ and Video 7; $n = 4$). Thus, Pacman activity was suppressed when the fiber was severed.

Kinetochores with severed K-fibers exhibit directionally unstable movements

Thus far, our experiments revealed that continuous K-fiber connection between a chromosome and a spindle pole was not required

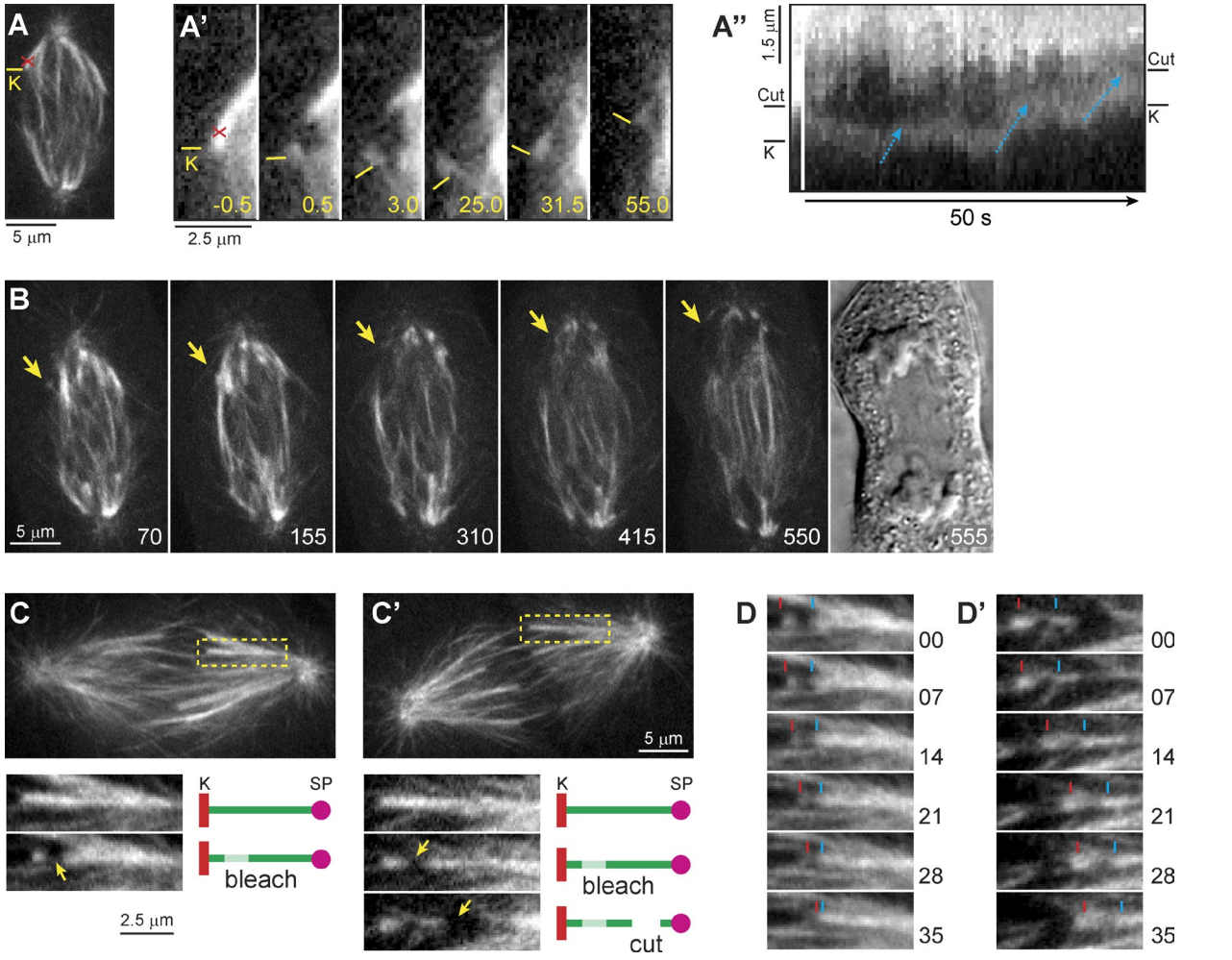

Figure 2. **Chromosomes lacking direct connection to the pole are not lost during anaphase.** (A–B) Behavior of a laser-severed K-fiber during anaphase in a PtK_2 cell. (A) Overview of the cell. (A′) Selected frames from time-lapse recording. Notice the change in orientation of the stub and its subsequent poleward movement (A′). (A″) Kymogram demonstrates that the K-fiber stub remains motionless for ∼15 s and then moves poleward in a series of rapid but brief movements (marked by blue arrows). Notice that the length of the stub remains constant throughout the experiment. (B) Longer-term time-lapse recording of the cell in A. Notice that the chromosome with severed K-fiber (arrow) ultimately incorporates into the forming daughter nucleus. K, estimated positions of the kinetochore; Cut, position of laser cut and minus end of the K-fiber stub. (C and D) Distinct mechanisms drive segregation of kinetochores with direct versus indirect attachments to the pole. (C) Creation of a bleached fiduciary mark on a continuous K-fiber with a 488-nm continuous wave laser beam. (C′) Combined bleach/sever approach to create a K-fiber stub with fiduciary mark. Notice that cells in C and C′ are at a similar stage of anaphase. (D) Movement of kinetochores with continuous K-fibers to the fiduciary mark indicates depolymerization of MT plus ends at the kinetochore (i.e., Pacman). (D′) Depolymerization of MT plus ends is not observed in laser-severed K-fibers. Instead the entire stub is transported poleward. Red lines denote positions of kinetochores and blue lines show bleached segments of MTs. Time in seconds.

for chromosome segregation. However, the velocity and pattern of poleward movement appeared to differ between chromosomes with intact versus severed K-fibers. Unfortunately, the abundance of MTs within the spindle complicates detailed quantitative analyses of the movement. Precise tracking, necessary for a more exact motion analysis, works best with discrete uniformly shaped objects. Therefore we conducted K-fiber severing experiments in human cells with fluorescently labeled kinetochores.

Laser ablation does not require that the target be fluorescently labeled. Although fluorescent tags help to delineate the target and determine its precise position (Magidson et al., 2007), unlabeled MTs are severed efficiently with 532-nm pulsed lasers used in our microsurgery workstation (Khodjakov et al., 1997b). Because of the stringent geometry of amphitelic attachment, the fiber should be severed when the laser beam is aimed <1 μm in front of the kinetochore. To ensure that K-fibers were not tilted in Z and to restrict chromosome movements to a single focal plane, these experiments were conducted in cells flattened to 3 μm (Fig. S3). Flattening allowed us to reconstruct trajectories of individual labeled kinetochores in RPE1 cells with high precision (10 frames/s in 108-nm pixel space).

Laser ablation of a single kinetochore on a bioriented chromosome invariably resulted in movement of the chromosome toward the spindle pole connected to the remaining kinetochore (Fig. 3, A and B). This behavior proved that, as in rounded cells (Rieder et al., 1995; Khodjakov et al., 1997a), in flattened cells a balance of forces acting on sister K-fibers is required for maintaining chromosome position at the spindle equator. In contrast, when one of the sister K-fibers was severed by laser pulses targeted 0.5–1.0 μm in front of a fluorescently labeled

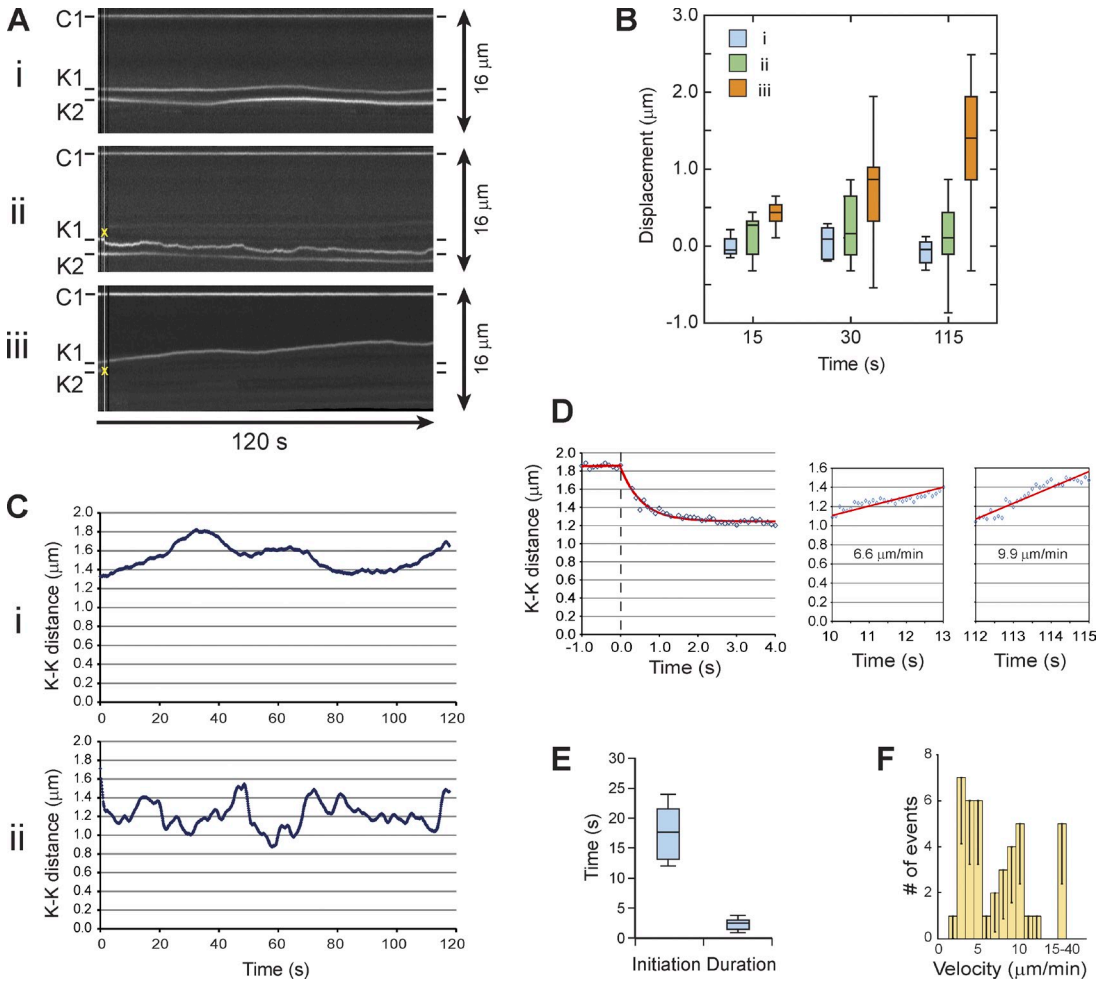

Figure 3. **Behavior of kinetochores with severed K-fibers in flattened RPE cells.** (A) High temporal-resolution (10 frames/s, 108-nm pixels) kymograms of kinetochore movements for a control chromosome (i), a chromosome with one intact (K2) and one severed (K1) K-fiber (ii), and a chromosome with a single kinetochore (K1). The sister kinetochore (K2) is ablated by laser (iii). Yellow crosses mark time and position of the laser beam. Notice that trajectories of kinetochores with intact K-fibers are smooth, whereas the kinetochore with severed K-fiber exhibits frequent poleward jumps. (B) Tukey plot characterization of the displacement from the original position for the classes of kinetochores presented in A. Control chromosomes (i) and chromosomes with severed K-fibers (ii) remain bioriented, whereas ablation of a single kinetochore results in a gradual displacement of the chromosome poleward (iii). (C) Dynamics of centromere stretching for the chromosomes shown in A (i and ii). Notice the difference between the relatively slow and smooth changes in the interkinetochore distance of the control chromosome (i) versus rapid transitions between stretching and relaxation of the centromere with one intact and one severed K-fiber. (D) Decrease in the interkinetochore distance induced by severing a K-fiber fits an exponential function, whereas restoration of centromere stretching is driven by rapid linear movements of the kinetochore attached to the severed K-fiber. Each panel presents a detailed view of short periods in C (ii). Time 0 marks laser irradiation. (E) Tukey plot characterization of the time from the K-fiber severing and initiation of the first poleward movement and the duration of the first poleward movement. (F) Distribution of kinetochore velocities during brief poleward movements of kinetochores with severed K-fibers. Error bars are 95% confidence intervals for binomial distribution.

kinetochore, the chromosome remained at the spindle equator (Fig. 3, A and B). However, this operation induced a prominent change in the pattern of the kinetochore's movement (Fig. 3, A and C).

K-fiber severing instantly relieved tension across the centromere as was evident from the exponential decrease of interkinetochore distance expected for elastic recoil (Fig. 3 D). The interkinetochore distance collapsed in <3 s and subsequently kinetochores with severed K-fibers exhibited a series of rapid albeit brief poleward movements (Fig. 3, C [ii] and D) that ultimately restretched the centromere. The first movement was initiated on average ~18 s after the fiber was severed and it lasted for ~3 s (Fig. 3 E and Table S1). Although this movement was sufficiently powerful to stretch the centromere, within a few seconds the interkinetochore distance always collapsed again because of a reversal in the direction of the kinetochore movement (Fig. 3 C, ii). The period of high-frequency directional instability of the kinetochore's movements varied in duration from 28 s to longer than the 2-min length of our recordings. The poleward velocity of kinetochores with severed K-fibers was also variable and could exceed 10 µm/min but only for a short time (Fig. 3, D and F).

Chromosomes lacking direct connection to the spindle pole exist in normal mitosis

High temporal-resolution recordings in flattened cells demonstrated that movements of kinetochores with severed K-fibers were directionally unstable. Rapid poleward jumps were interspersed

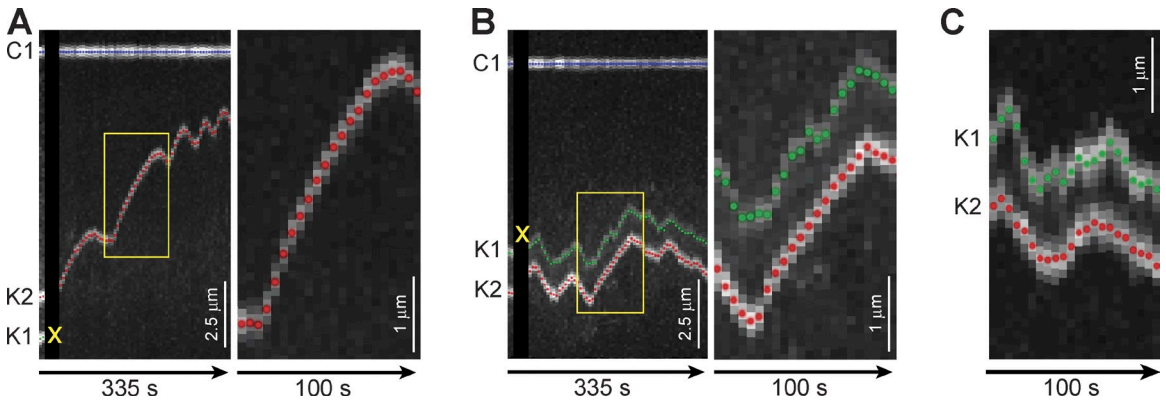

Figure 4. **Directionally stable versus unstable kinetochore trajectories in rounded RPE1 cells.** (A) Ablation of a single kinetochore (K1) on a bioriented chromosome results in a directionally stable movement of the remaining kinetochore (K2) toward the centrosome (C1). Only low-frequency oscillations (1–2 min periodicity) are evident in the K2 trajectory. (B) Sister kinetochores with laser-severed (K1) versus intact (K2) K-fibers exhibit distinctly different trajectories. Notice that K2 trajectory is smooth, whereas K1 exhibits rapid directional instability. In spite of the severed connection to one spindle pole, the chromosome remains at the spindle equator. Yellow crosses mark the laser beam. Insets are shown at higher magnification. (C) Example of sister kinetochores (K1 and K2) with distinctly different trajectories in an unperturbed RPE1 cell. Notice the high-frequency directional instability in the trajectory of K1.

with brief periods of away-from-the-pole movements. We sought to determine whether the same pattern can be detected in nonflattened RPE1 cells where the temporal resolution of recordings is limited by the necessity to collect Z-series instead of individual focal planes at every time point. Chromosomes with clearly stretched centromeres and coplanar sister kinetochores positioned near the middle focal plane of the spindle (determined by the positions of centrosomes) were chosen for these operations to ensure that the K-fibers were minimally tilted in Z and thus were reliably severed.

When one of the sister kinetochores was ablated, the chromosome became monooriented toward the spindle pole connected to the remaining kinetochore and the trajectory of poleward movement did not exhibit high-frequency directional instability (Fig. 4 A). In contrast, when a K-fiber was severed by aiming the laser ∼0.5 µm in front of the kinetochore, the chromosome remained near the spindle equator. However, trajectories of the sister kinetochores now differed dramatically. Kinetochores with intact K-fibers continued to move smoothly whereas the kinetochores with severed K-fibers exhibited characteristic brief (5–10-s) poleward jumps (Fig. 4 B). Interestingly, similar asymmetry in the behavior of sister kinetochores was occasionally detected in control RPE1 cells that were not exposed to laser irradiation (Fig. 4 C). This observation prompted us to investigate whether kinetochores lacking direct connections to the spindle poles exist in normal human mitosis.

Detailed 3D spinning-disc confocal immunofluorescence examination of metaphase and early anaphase cells with labeled centrosomes, kinetochores, and MTs revealed the presence of short K-fibers that did not extend to a spindle pole. Instead, the minus ends of these K-fibers appeared to terminate in the vicinity of other K-fibers and/or nonkinetochore MTs (Fig. 5, A and B). At least one such putative short K-fiber was found in every RPE1 cell examined ($n > 20$). However, the exact number of these bundles per cell could not be determined because of limitations inherent in conventional LM.

The high density of MTs and their complex 3D distribution are major impediments to tracing MT bundles within the spindle. The defocused light emitted by MTs outside of the focal plane as well as the inadequate resolution in Z (along the optical axis of the microscope) make it difficult to determine whether a K-fiber truly terminates in the vicinity of another MT bundle or whether it simply becomes indistinguishable in the high-intensity fluorescence background. To overcome these problems we traced K-fibers in three cells reconstructed via array tomography (Micheva and Smith, 2007). RPE1 cells, stained for MTs, were embedded in resin and serially cut into 80-nm (one early anaphase cell) or 200-nm (two metaphase cells) sections. Fluorescence images were recorded individually for each section, which eliminated contamination of the images with blur. In these reconstructions, the minus ends of three to four K-fibers in each cell were found terminating at a short distance from the kinetochores in the vicinity of another K-fiber or a MT bundle (Fig. 5 C and Video 8).

Short K-fibers were also observed in cells that were briefly exposed to cold before fixation (0°C, 2–4 min). This treatment induced a rapid depolymerization of nonkinetochore MTs, thus making the K-fibers more prominent. Several clear examples of K-fibers lacking direct connection to the pole were found in every metaphase and early anaphase RPE1 cell with this technique (Fig. S4, A and B; $n > 20$). Multiple short fibers were also detected in every hyper-triploid human U2OS cell (Fig. S4 C, $n > 20$), suggesting that the phenomenon is not specific to RPE1 cells.

A limitation of all approaches that involve immunostaining is that cells are lysed to enable antibody penetration. Considering the high lability of spindle MTs, it is formally possible that some changes in the distribution of MTs occur during lysis before the cell is fully fixed. Therefore, we searched for the presence of short K-fibers in nonlysed glutaraldehyde-fixed cells with GFP-labeled MTs. Two examples of apparent short K-fibers were identified in three PtK_2 cells. We traced the individual MTs within these short K-fibers in correlative 150-nm serial EM sections (Fig. 6 A). These reconstructions revealed that MT distribution at the minus ends of short K-fibers resembled that of laser-severed K-fibers (compare Fig. 6 A with Fig. 1, C and D): the minus ends of some of the MTs within the short K-fiber

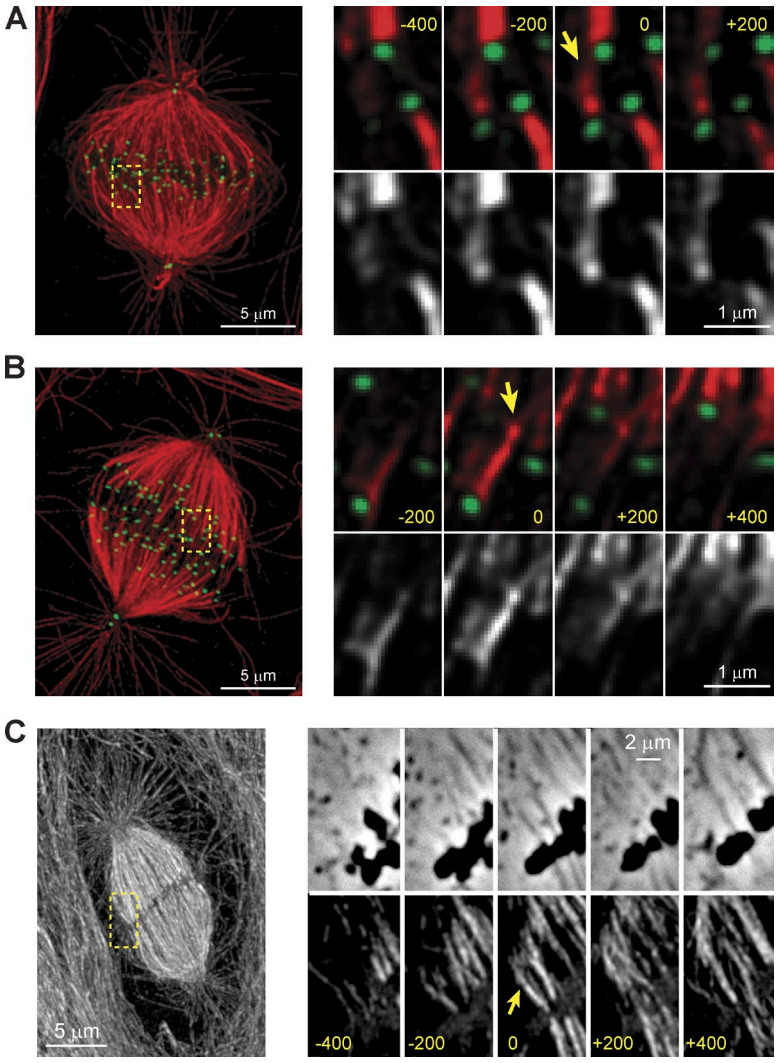

Figure 5. **K-fibers lacking direct connection to the spindle pole visualized by confocal LM and array tomography.** (A) Metaphase spindle in RPE1 cell (maximal-intensity projection). Series of individual focal planes separated by 200 nm are shown for the boxed area. Notice a short bundle of MTs that emanates from one kinetochore. This bundle terminates in the vicinity of a different kinetochore (arrow) and appears to form a side connection to this kinetochore's K-fiber. (B) As in A, but the cell is in early anaphase. Red, MTs (also shown in grayscale); green, kinetochores (CenpA-GFP) and centrioles (Centrin-GFP). (C) Metaphase RPE1 cell reconstructed via array tomography (see Materials and methods). Left panel presents a maximal-intensity projection of the entire reconstructed volume. Notice the high density of MTs in cells that become apparent with this approach. Consecutive 200-nm sections are shown at higher magnification for the boxed area. Arrows indicate the termination of short MT bundles emanating from kinetochores.

were in close proximity of other spindle MTs. Additional MT contacts appeared to exist along the length of the short fiber (Fig. 6 A). Finally, putative short fibers were identified in correlative LM/EM analyses of two fully assembled metaphase RPE1 cells with GFP-labeled kinetochores. The locations of all kinetochores were estimated from 3D fluorescence images and the MTs in the vicinity of each kinetochore were traced in corresponding EM sections. Three K-fibers whose minus ends appeared to terminate at another K-fiber instead of extending to a pole were found (Fig. 5 C). Thus, the structural data are consistent with the notion that some chromosomes in fully assembled spindles lack direct K-fiber connections to the spindle poles.

Similar to that of laser-severed K-fibers, the minus ends of the naturally occurring short K-fibers were usually decorated with small amounts of NuMA (Fig. S5). This observation, combined with the similarity in MT distribution near the minus ends of natural and laser-severed short K-fibers, suggested that a common mechanism is responsible for the positioning and segregation of chromosomes not directly attached to the spindle poles.

Poleward movements of indirectly attached kinetochores are driven by cytoplasmic dynein

Brief high-velocity poleward jumps, characteristic of kinetochores with severed K-fibers, were occasionally seen in the trajectories of kinetochores in control cells (Fig. 4 C). To estimate the frequency of these events we followed individual pairs of sister kinetochores at 5-s intervals (Magidson et al., 2011) for >10 min before anaphase onset and throughout anaphase. Based on the results of the laser microsurgery experiments (Fig. 3 F), the poleward movements were categorized as fast when momentous velocity exceeded 5 µm/min.

Fast movements were observed infrequently (<3% of cumulative time) during both metaphase (the last 10 min before the onset of anaphase) and anaphase. To compare individual trajectories we calculated the percentage of time when a particular kinetochore moved faster than 5 µm/min. The great majority of kinetochores in RPE1 cells (43/46 during metaphase and 28/30 during anaphase) continuously moved at slower rates or exhibited only occasional individual jumps that accounted for <5% of the total recording time. However, fast poleward movements

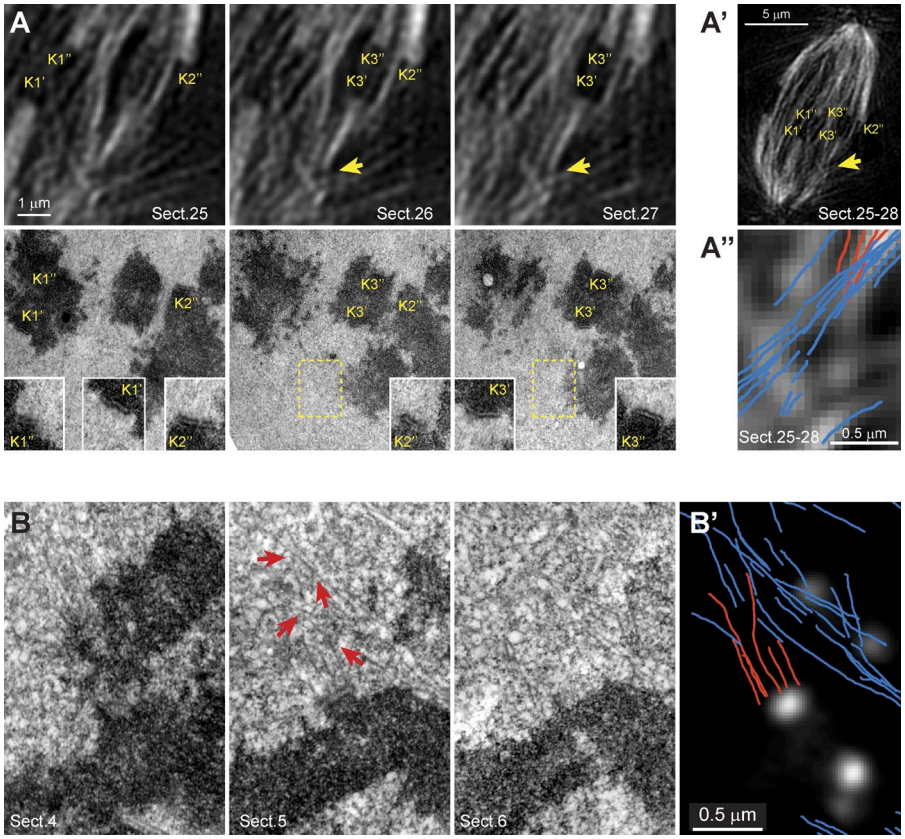

Figure 6. **K-fibers lacking direct connection to the spindle pole visualized by correlative LM/EM.** (A) Sequential focal planes and corresponding 150-nm EM sections of a PtK2 cell with GFP-labeled MTs. All kinetochores present in this part of the cell are shown at twofold higher magnification in insets. K-fibers attached to K1′, K1′′, K2′′, and K3′′ can be traced continuously to the spindle poles (A′). In contrast, K-fiber attached to K3′ appears to terminate ∼2.5 µm from the kinetochore (arrows). (A′′) tracing of individual MTs superimposed on GFP fluorescence in the area boxed in A. Notice that minus ends of K-fiber MTs (orange) are in close proximity to a MT bundle that was not traced to a particular kinetochore (i.e., nonkinetochore MT bundle). (B) Consecutive 80-nm EM sections from a full series of a metaphase RPE1 cell. (B′) Traces of MTs in the vicinity of kinetochores superimposed on the corresponding fluorescence planes. Notice short MTs that extend from a kinetochore to wall of MTs in a neighboring K-fiber. Arrows denote potential contacts between MTs.

were more frequent in a low number of individual trajectories (Fig. 7 A). Exaggerated directional instability was particularly prominent in the trajectories of some kinetochores during anaphase. These chromosomes (2/30 in RPE1 cells) exhibited periods of rapid poleward movement intermittent with stops and movements away from the pole. The poleward velocity of these chromosomes exceeded 6 µm/min for periods of up to 20 s long (Fig. 7 B). The same pattern of directionally unstable kinetochore movements was observed in U2OS cells (Fig. 7 A). During metaphase, the frequency of jumps in U2OS cells was similar to that in RPE1 cells. However, rapid directional instability during anaphase was more frequent in U2OS cells (Fig. 7 A).

The high momentous velocity during poleward jumps suggested that directionally unstable movements are driven by a fast minus end–directed MT motor. Previous work has implicated cytoplasmic dynein in the poleward transport of preformed K-fibers and nonkinetochore MTs (Rusan et al., 2002; Tulu et al., 2003; Khodjakov et al., 2003; Maiato et al., 2004). Therefore, we investigated whether inhibition of dynein activity suppresses directional instability in the kinetochore trajectories.

Because of the essential role of dynein in the formation of spindle poles, a complete or even a significant partial inhibition of this motor grossly perturbs the spindle architecture. Therefore, we focused our analyses on mild suppression of dynein activity by low concentrations of Ciliobrevin, a cell-permeable chemical inhibitor of dynein (Firestone et al., 2012).

A high concentration of Ciliobrevin (50 µM) has been shown to inhibit dynein to the extent that disrupts spindle bipolarity (Firestone et al., 2012). We found that in cells treated with 10 µM Ciliobrevin for 2 h, the spindle remained bipolar and chromosomes congressed into a tight metaphase plate (Fig. 7 C). However, a noticeable gap appeared between the minus ends of spindle MTs and the centrosome. The width of the spindle pole, measured as the distance between the minus ends of outmost peripheral K-fibers, increased from 1.7 ± 0.4 to 2.6 ± 0.5 µm in RPE1 cells ($n = 30$) and from 1.5 ± 0.3 to 3.6 ± 0.9 µm ($n = 30$) in U2OS cells. This increase indicated that the pole-focusing mechanisms were not fully functional in Ciliobrevin-treated cells. Further, the spindle was surrounded by individual MTs that extended toward the periphery of the cell. This change in MT distribution was consistent with the notion that dynein transports distal ends of MTs/MT bundles inwards into the spindle (Khodjakov et al., 2003; Tulu et al., 2003). Thus, we concluded that 10 µM Ciliobrevin partially inhibits dynein activity in human cells.

Treatment of cells with 10 µM Ciliobrevin for 2 h effectively eliminated rapid directional instability in the kinetochore trajectories. Only one jump exceeding the 5-µm/min velocity was observed in the recordings of Ciliobrevin-treated RPE1 and U2OS cells during metaphase (46 10-min-long trajectories for each cell line) or anaphase (32 5-min-long trajectories for each line). The poleward movements during anaphase were consistently smooth, without significant pauses or directional reversals (Fig. 7 D). The mean poleward velocity during anaphase (1.7 ± 0.1 µm/min [$n = 30$]) was also slower than that in untreated cells (2.3 ± 0.3 µm/min [$n = 30$], $P = 0.003$), consistent with a previous study showing that depletion of kinetochore-associated dynein reduced the velocity of anaphase chromosome motion up to 40% (Yang et al., 2007).

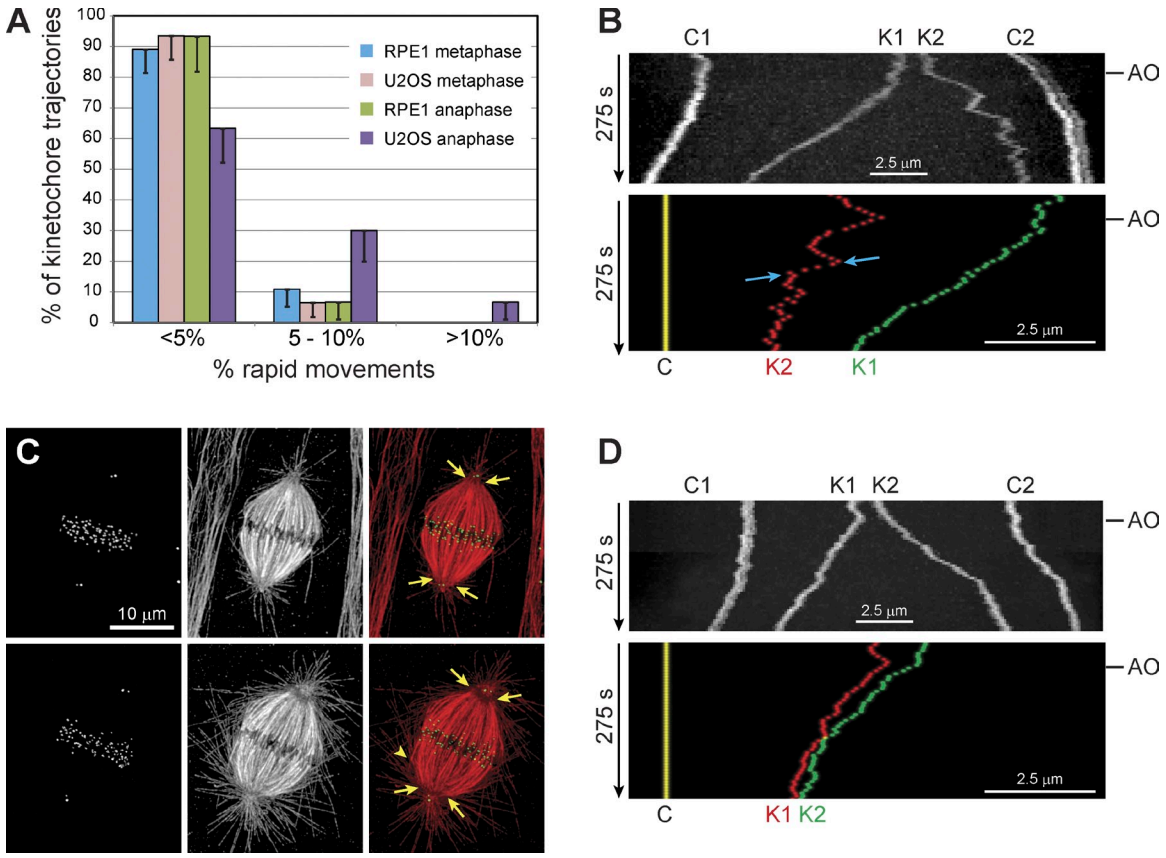

Figure 7. **Partial inhibition of dynein suppresses rapid directional instability in kinetochore trajectories.** (A) Frequency of fast jumps in kinetochore trajectories. Error bars are 95% confidence intervals for binomial distribution. (B) Example of kinetochore movement patterns during anaphase in an RPE1 cell. K1 moves monotonically (directionally stable), whereas K2 exhibits periods of rapid poleward movement intermittent with directional reversals. Arrows mark periods when poleward velocity exceeds 6 µm/min. Top panel presents a raw kymogram. In the bottom panel, movements of each kinetochore are shown with respect to its connected centrosome. C1 and C2, centrosomes; K1 and K2, sister kinetochores. (C) Spindle organization in control (top row) versus 10 µM Ciliobrevin-treated RPE1 cells. Notice separation of the centrosomes from the spindle poles, widening of the spindle poles (arrows), and exaggerated presence of peripheral MTs in the drug-treated cell. Arrowhead denotes a short K-fiber, not attached to the spindle pole in a Ciliobrevin-treated cell. (D) Example of kinetochore trajectories in an RPE1 cell treated with 10 µM Ciliobrevin for 2 h. Notice decreased poleward velocity (compare slope of the trajectories in B) and monotonous (directionally stable) pattern of kinetochore movements.

The stubs of laser-severed K-fibers in PtK_2 cells treated with 10 µM Ciliobrevin were able to interact with the neighboring MTs and be transported poleward. However, the mean time from fiber severing to the initiation of poleward movement increased significantly ($P < 0.004$) from 5.3 ± 1.0 ($n = 19$) to 18.7 ± 3.6 s ($n = 19$), whereas the mean poleward velocity decreased only slightly from 4.7 ± 0.7 to 3.5 ± 0.4 µm/min. This decrease in the mean value was not statistically significant ($P = 0.06$, $n = 19$), consistent with the notion that dynein was only partially inhibited.

Discussion

A common theme emerging from recent studies on the mechanisms of cell division is that every step of chromosome segregation can be achieved via multiple parallel pathways. For example, K-fibers are known to form via direct capture of astral MTs (Hayden et al., 1990; Tanaka et al., 2005) as well as by outgrowth of MT bundles from the kinetochores followed by dynein-driven poleward transport of these bundles (Khodjakov et al., 2003; Maiato et al., 2004; Tulu et al., 2006). Congression of chromosomes onto the metaphase plate is driven by several mechanisms including CenpE-mediated gliding of unattached kinetochores alongside MT bundles (Kapoor et al., 2006; Kim et al., 2008; Cai et al., 2009) and dynein-mediated transport of chromosomes with preformed K-fibers (Khodjakov et al., 2003; Maiato et al., 2004). Here we present evidence that dynein-mediated poleward transport of K-fibers can drive the segregation of individual chromosomes during anaphase in mammalian cells (Fig. 8). This mechanism is principally different from the Pacman activity that propels the majority of mammalian chromosomes during anaphase. The hallmark of Pacman is that chromosome movement is coupled with depolymerization of K-fiber MTs at the kinetochore (Gorbsky et al., 1987; Desai et al., 1998; LaFountain et al., 2012). In contrast, we find that the MT ends at the kinetochore become stable when the fiber is severed.

The cessation of MT depolymerization at the kinetochore upon the detachment of the K-fiber minus end from the pole implies that Pacman activity is regulated at the level of individual kinetochores. This regulation somehow distinguishes between intact K-fibers that are attached to a pole and short K-fibers that lack this attachment. The exact trigger for Pacman shutdown

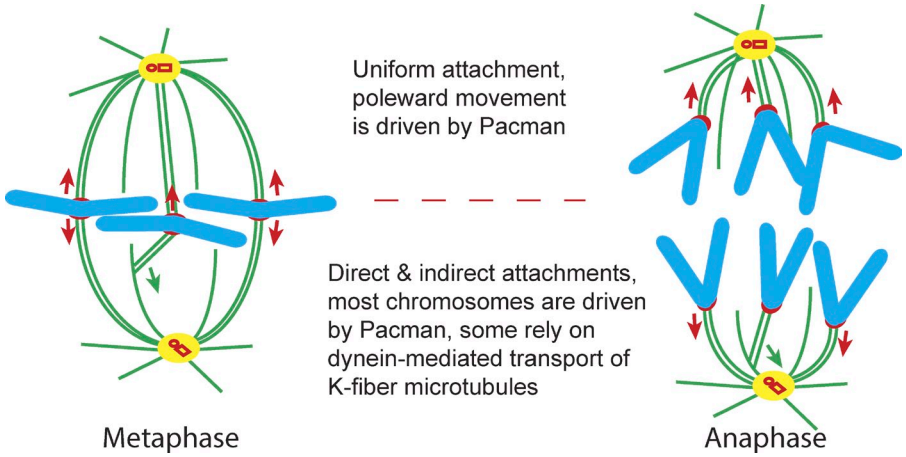

Figure 8. **Alternative mechanisms for chromosome segregation in mammalian mitosis.** Chromosomes that fail to establish direct connections with the spindle poles nevertheless maintain their position near the spindle equator and segregate during anaphase via dynein-mediated force that acts upon a short K-fiber attached to the kinetochore. Poleward movements of these chromosomes are not coupled with depolymerization of K-fiber MTs at the kinetochore (Pacman mechanism). Instead the entire short fiber with the attached kinetochore is transported toward the spindle pole.

remains unknown; however, it is tempting to speculate that this switch involves tension within the K-fiber. A role for tension in regulating Pacman activities has been demonstrated in crane fly spermatocytes (LaFountain et al., 2011, 2012). In this system, Pacman activity is normally suppressed and segregation is achieved by a pulling force on the K-fiber. However, when tension in the system is relieved kinetochores suddenly engage Pacman (LaFountain et al., 2012).

Establishing direct connections between spindle poles and the large number of chromosomes in the crowded volume of a mammalian cell is a formidable steric problem. As the minus ends of preformed K-fibers are transported poleward, their movements are likely to be obstructed by other K-fibers and nonkinetochore MT bundles. Resolving the entanglement would not be possible without severing at least some of the MTs and therefore sporadic detachment of individual K-fibers from the spindle pole is likely. Our experiments reveal that such an accidental detachment does not automatically imply that the chromosome will be lost. During metaphase, accidental detachments appear to be repaired in two stages: (1) Dynein-mediated force applied to the K-fiber stub allows the chromosome to maintain its position and also stretches the centromere so that K-fiber MTs are not actively destabilized by the Aurora B–mediated system responsible for the correction of erroneous attachments (Lampson and Cheeseman, 2011); and (2) gradual growth of the K-fiber stub caused by continuous polymerization of MTs at the kinetochore eventually delivers the minus ends of the broken K-fiber to the pole (Maiato et al., 2004). The growing stub would be positioned alongside other K-fibers, which decreases the likelihood of additional entanglements. However, complete regrowth of a K-fiber can take up to 5–8 min in a typical spindle. Further, the presence of short K-fibers cannot be detected by the spindle assembly checkpoint as the kinetochores remain attached and under full tension. Therefore, the ability of dynein-mediated transport to propel the chromosome all the way to the spindle pole during anaphase becomes essential for preventing the loss of chromosomes with short K-fibers.

Our observation that chromosomes with K-fibers severed during metaphase remain at the spindle equator is consistent with similar work in various cell types (Spurck et al., 1990; Maiato et al., 2004, 2005; Sheykhani et al., 2013). However, it seems to contradict a recent finding that in human HeLa cells chromosomes with severed K-fibers move toward the spindle pole attached to the intact K-fiber (Dick and Gerlich, 2013). This inconsistency may be superficial because of the difference in how exactly the cuts were performed. In our operations, a highly focused beam was used to sever a single fiber with minimal damage to the adjacent MTs. Under this experimental design, K-fiber stubs could rapidly attach to the unperturbed MTs. Yet, in ∼5% of the operations we observed interactions between the stub and MTs from the opposite spindle pole followed by reorientation of the stub to that pole. This process converted an amphitelic attachment into a syntelic one. Expectedly, the syntelic chromosome moved to the opposite spindle pole (Fig. S1 C). In contrast, Dick and Gerlich (2013) used a scanning laser beam to cut across a large part of the spindle, severing not only a K-fiber but also most of the adjacent MTs as well. As a result, the probability of K-stub reorientation would increase, explaining why chromosome movement to the opposite spindle pole was often observed. The subsequent destabilization of the tensionless syntelic attachments is also consistent with the recruitment of the checkpoint proteins to monooriented chromosomes observed in the Dick and Gerlich (2013) experiments.

In current models, spindle organization is envisioned as a confederation of K-fibers: each K-fiber connects a chromosome directly to a spindle pole so that all chromosomes interact with the poles in in the same fashion (Walczak et al., 2010; McIntosh et al., 2012). Our experiments suggest that this view is an oversimplification. K-fibers that fail to connect a chromosome directly to a spindle pole or lost such a connection during metaphase use dynamic attachments to other K-fibers and/or nonkinetochore MTs to segregate. Therefore, the density of MTs and the activity of dynein (and potentially other molecular motors with minus end directionality; Kleylein-Sohn et al., 2012) become important factors in ensuring proper chromosome segregation. Our observations on the segregation of chromosomes not directly connected to a pole are consistent with previous studies on the continuation of anaphase movement upon the separation of the polar region from the rest of the spindle via micromanipulation and UV-irradiation experiments (Nicklas, 1989; Spurck et al., 1990). Mechanical linkages between adjacent K-fibers are reported in insect spindles during meiosis (Nicklas et al.,

1982). Therefore, the idea that some K-fibers in mammalian cells attach to surrounding MTs instead of extending all the way to the spindle pole is consistent with observations in other systems. Unfortunately, because of the high density of MTs and the roundness of cells during mitosis, the detection of these short fibers remains challenging even with modern imaging. Each of the approaches used in our work to detect short K-fibers (confocal microscopy, array tomography, and serial-section EM reconstructions) is not perfect. However, the fact that short K-fibers are consistently detected by this range of techniques with nonoverlapping limitations makes the existence of these structures certain. It is tempting to speculate that the proportion of chromosomes with indirect connections varies among different cell types. Such variability would potentially explain why certain cell types are more sensitive to the inhibition of dynein activity.

Materials and methods

Cell culture and live-cell imaging

Creation of hTERT RPE1 (Takara Bio Inc.) clones that stably express CenpA-GFP, CenpA-PAGFP, and centrin1-GFP has been detailed elsewhere (Magidson et al., 2011). In brief, all fluorescent proteins were fused to full-length human proteins and introduced via lentivirus transfection in the Lentilox3.1 vector under the nonregulated CMV promoter. The same viruses were used to infect populations of U2OS cells (ATCC). Individual clones with fluorescently labeled kinetochores and centrioles were obtained by two rounds of limited-dilution cloning from the infected populations. PtK_2 cells expressing GFP–α-tubulin have been described elsewhere (Khodjakov et al., 2003). In brief, the cells were electroporated with a commercial full-length human eGFP–α-tubulin plasmid (CMV promoter; Takara Bio Inc.) and individual clones were isolated by two rounds of limited-dilution cloning in the presence of G418. RPE1 cells expressing YFP–α-tubulin (Holland et al., 2010) were provided by A. Holland (Johns Hopkins University School of Medicine, Baltimore, MD). To generate these cells, RFP-tagged histone H2B (H2B-mRFP) and EYFP-tubulin were cloned into the pBabe backbone under control of the gag promoter. Constructs were introduced into Plk4+/WT RPE1 cells using retroviral delivery as described previously (Shah et al., 2004). Stable integrates were selected in 5 µg/ml puromycin and 10 µg/ml blasticidin S and single clones were isolated using fluorescence-activated cell sorting (FACSVantage; BD).

All human cells were grown in DMEM and PtK_2 cells were grown in 1:1 mixture of Ham's F12 and DMEM media at 37°C and 5% CO_2. In all cases, media was supplemented with 10% FCS (Life Technologies). For live-cell imaging, cells grown on coverslips for 24–48 h were mounted in Rose chambers containing CO_2-independent medium (Life Technologies) supplemented with 10% FCS and antibiotics (penicillin and streptomycin). The chambers were maintained at 37°C on the microscope stage.

Laser microsurgery, photoactivation, photobleaching, and motion analyses

Our laser microsurgery/photobleaching/photoactivation workstation is detailed elsewhere (Magidson et al., 2007). Laser microablation was achieved with a brief (~200-ms) series of 532-nm (0.56-ns, 250-Hz) pulses generated by a Q-switched Nd:YAG laser (Teem Photonics). 488-nm (Ar^+ laser; Laser Physics) and 405-nm (CUBE 405-50FP diode laser; Coherent) continuous-wave laser beams were used for marking individual GFP–α-tubulin–labeled K-fibers and photoactivation of CenpA-PA-GFP–labeled kinetochores, respectively. Collimated laser beams were steered through a dedicated epi-port of a microscope (TE-2000E PFS; Nikon) and focused by a 100× Plan Apochromat, NA 1.4 oil-immersion objective lens (Nikon). Images were recorded in spinning-disk confocal mode (CSU-10; Yokogawa Electric Corporation) on a back-illuminated charge coupled device (CCD) camera (Cascade 512B EM; Photometrics). The system was controlled by IPLab software (Scanalytics).

In most time-lapse recordings, multiple (5–17) focal planes separated by 500 nm were collected at each time point every 5 s. For higher temporal resolution recordings, a single focal plane was recorded at ≤1-s intervals. For live-cell imaging, cells were mounted in Rose chambers containing CO_2-independent medium and maintained at 37°C at all times.

10–frame-per-second trajectories of kinetochores were obtained under conditions that prevented rounding of cells during mitosis. This was achieved by placing a coverslip with microfabricated feet of known height (3 µm) on top of the coverslip with the growing cells. The distance between coverslips was maintained with negative pressure using a vacuum pump (Le Berre et al., 2012).

Movements of kinetochores and/or MTs were analyzed in kymograms. All kymograms were created from images that were rotationally aligned at every time point to fix the orientation of the axis of spindle (for kinetochore tracking, see Video 9) or the orientation of the K-fiber of interest (for tracking K-fiber stubs or for determination of flux values, see Video 10). In many cases, images of each time point were also shifted to fix the position of one of the centrosomes or one of the kinetochores. This processing allowed us to illustrate changes in relative positions of multiple objects with respect to a pseudo-stationary reference object (see Fig. 6, B and D).

All image processing was done in MatLab (MathWorks) and ImageJ (National Institutes of Health). Calculations and statistical analyses were done either in MatLab or Microsoft Excel. Distances between diffraction-limited objects (kinetochores and centrioles) were measured with subpixel precision by fitting each object to a Gaussian function. The fit was performed with open-source MatLab scripts developed by O'Haver (2009). In experiments with labeled MTs the ends of K-fibers were tracked manually using standard ImageJ functions and plugins.

Mean poleward velocities of chromosomes with laser-severed K-fibers were measured for the 6-s period from the initiation of poleward motion. Mean velocities of oscillating bioriented chromosomes were also determined for 6-s periods during the phase of stable unidirectional movement. The values are reported in the text as mean ± SEM. Differences between mean values were assessed by one-tailed Student's *t* test.

Immunofluorescence preparations imaging of fixed cells

For conventional immunofluorescence and array tomography, cells were lysed in warm PEM buffer (100 mM Pipes, pH 6.9, 2.5 mM EGTA, and 5 mM $MgCl_2$, pH6.9) supplemented with 0.5% Triton X-100 for 1 min before fixation with 1–2% glutaraldehyde for 10 min in PEM. For correlative live-GFP/fixed immunofluorescence analyses, cells were lysed concurrently with fixation in 1% Triton X-100 plus 1% glutaraldehyde solution in PEM buffer (20 min). MTs were visualized with DM1α monoclonal anti–α-tubulin antibody (Sigma-Aldrich). Hoechst 33343 was used to stain DNA (chromosomes). NuMA was visualized with a rabbit antibody (Gaglio et al., 1995) provided by D. Compton (Dartmouth Medical School, Hanover, NH).

Multicolor Z-series of immunostained cells were collected in either spinning disc confocal or wide-field fluorescence modalities. Spinning disc images were recorded on Revolution (Andor Technology) with a 100× NA1.4 Plan Apochromat VC lens (Nikon) and GSU-22 scanner (Yokohama). Images were captured with the iXon-885 EM CCD camera (Andor Technology) at 55-nm X-Y pixel size. The system was controlled by iQ2 imaging software (Andor Technology). Wide-field images were recorded on a DeltaVision imaging system (Applied Precision) with a 100× NA1.35 lens (Olympus). The images were captured with the CH-350 CCD camera (Photometrics) at 69-nm X-Y pixel size. All images were deconvolved with the SoftWoRx 5.0 deconvolution software (Applied Precision) and objective lens-specific point spread functions.

Correlative EM

Cells were fixed in 2.5% glutaraldehyde (Sigma-Aldrich) in PBS (pH 7.4–7.6). Differential interference contrast and fluorescence images were acquired at 0.1-µm Z steps through the entire cell volume immediately after fixation. Post-fixation, embedding, and sectioning were done as previously described (Rieder and Cassels, 1999). In brief, cells were post-fixed with 1% aqueous OsO_4, dehydrated in a series of alcohol, embedded in Epon812. Serial thin sections (80 or 150 nm), and imaged on either a 910 (Carl Zeiss) or 1400 microscope (JEOL) operated at 80–100 kV. Correlation of conspicuous morphological features between differential interference contrast and EM images was used to match the orientation and Z positions for individual focal planes and then fluorescence images were overlaid on the EM reconstruction to determine exact positions of kinetochores.

Array tomography

Cells were fixed and processed as for conventional immunofluorescence and then embedded in Lowicryl resin following conventional protocols. The resin was UV polymerized at −25°C for 48 h (Kukulski et al., 2011). Continuous ribbons of serial 80- or 200-nm sections were adhered to square 9 × 9 #1.5 coverslips, dried, and mounted in glycerol. Each section was imaged independently in spinning disc confocal mode as for conventional

immunofluorescence analyses. Phase-contrast images were also recorded for each section. As both fluorescence and phase-contrast images were recorded on the same CCD camera, these images were inherently coregistered, which facilitated subsequent reconstruction of the spindle. Sequential sections were initially aligned by using large features (chromosomes and adjacent cell nuclei) prominent in phase-contrast images. This primary alignment was subsequently refined by enforcing continuity of astral MTs that traversed multiple sections.

Dynein inhibition

Ciliobrevin D ((E)-2-(7-chloro-4-oxo-3,4-dihydroquinazolin-2(1H)-ylidene)-3-(2,4-dichlorophenyl)-3-oxopropanenitrile) and Ciliobrevin 83 ((E)-2-(7-chloro-4-oxo-3,4-dihydroquinazolin-2(1H)-ylidene)-3-(2,4-dibromophenyl)-3-oxopropanenitrile) were the two Ciliobrevin analogues used in this study. Ciliobrevin 83 varies from Ciliobrevin D in that it has a 2,4-dibromophenyl ring in place of the 2,4-dichlorophenyl group of Ciliobrevin D. Ciliobrevin D and 83 have similar dynein inhibitory activity in in vitro MT gliding assays. The effects of both forms of Ciliobrevin on spindle architecture and chromosome velocities are also similar.

Ciliobrevin 83 was synthesized as follows: (a) 2-cyanothioacetamide (1.2 equivalents) was added to an ethanolic solution of sodium ethoxide and bromoethane (1.3 equivalents). This mixture was stirred overnight at 50°C. After cooling, this solution was added to 2-amino-4-chlorobenzoic acid (1; 1.9 mmol, 1 equivalent) in 3 ml of ethanol. This mixture was stirred at 50°C overnight. Upon cooling, 3% NaOH (aq) was added and a precipitate formed. The precipitate was recovered by vacuum filtration and determined to be (*Z*)-2-(7-chloro-4-oxo-3,4-dihydroquinazolin-2(1*H*)-ylidene)acetonitrile (2; 190 mg, 22% yield), which was used without further purification. (b) 2 (200 mg, 0.45 mmol, 1 eq) was dissolved in 2 ml dioxane with triethylamine (1.25 equivalents). 2,4-dibromobenzoyl chloride (305 mg, 1.1 equivalents in 1ml dioxane, prepared by heating 2,4-dibromobenzoic acid in thionyl chloride for 2 h at 50°C followed by rotary evaporation) was added and the mixture was heated at reflux overnight. The reaction was cooled and a precipitate formed. The solvent was removed by filtration and the precipitate was washed sequentially with methanol, water, methanol, and dichloromethane to yield Ciliobrevin 83 (56 mg, 12% yield) as an orange-brown solid. Observed chemical shifts in proton nuclear magnetic resonance (1-proton nuclear magnetic resonance, 400 MHz; solvent: DMSO-d6) were as follows: δ 8.04 (doublet, 1 proton, coupling constant J = 8.5 Hz), 8.00 (singlet, 1 proton), 7.90 (singlet, 1 proton), 7.72 (doublet, 1 proton, J = 7.8 Hz), 7.49 (doublet, 1 proton, J = 8.2 Hz), and 7.40 (doublet, 1 proton, J = 8.03 Hz). Using electrospray ionization mass spectrometry, an M/z of 480.07 was observed (molecular mass/charge + proton). The calculated exact mass is 479.88.

Ciliobrevin D was prepared according to the aforementioned procedure but 2,4-dichlorobenzoyl chloride replaced the 2,4-dibromobenzoyl chloride in step b. Nuclear magnetic resonance and mass spectrometry data of the final product were consistent with those previously reported by Firestone et al. (2012).

Illustrations

For illustrations, ImageJ was used to scale images to the final size at 300 DPI without interpolation. Brightness and contrast of the final images were adjusted in Photoshop CS4 (Adobe Systems, Inc.) and figures were assembled in Illustrator CS4 (Adobe Systems, Inc.).

Online supplemental material

Figs. S1 and S2 present MT flux in individual K-fibers and additional examples of laser-severed K-fiber behavior in PtK_2 cells. Fig.S3 characterizes mitosis in flattened RPE1 cells. Fig. S4 illustrates detection of short K-fibers by confocal microscopy in cold-treated RPE1 and U2OS cells. Fig. S5 illustrates association of NuMA with the minus ends of short K-fibers. Videos 1–8 are complete recordings used to select the frames presented in figures. Videos 9 and 10 illustrate alignment techniques used for generation of kymograms. Table S1 shows the results of laser microsurgery experiments. Online supplemental material is available at http://www.jcb.org/cgi/content/full/jcb.201401090/DC1.

Electron microscopy was enabled by the use of the Wadsworth Center's Electron Microscopy Core Facility. We thank Drs. Duane Compton and Andrew Holland for their generous gifts of antibodies and cells. Special thanks to Dr. Sophie Dumont for sharing data before publication and insightful comments on the manuscript. We appreciate stimulating discussions with Dr. Michael Koonce that significantly influenced this work.

This work was supported by National Institutes of Health grant GM059363 to A. Khodjakov.

The authors declare no competing financial interests.

Submitted: 21 January 2014
Accepted: 16 June 2014

References

Cai, S., C.B. O'Connell, A. Khodjakov, and C.E. Walczak. 2009. Chromosome congression in the absence of kinetochore fibres. *Nat. Cell Biol.* 11:832–838. http://dx.doi.org/10.1038/ncb1890

Church, K., and H.P. Lin. 1982. Meiosis in *Drosophila melanogaster*. II. The prometaphase-I kinetochore microtubule bundle and kinetochore orientation in males. *J. Cell Biol.* 93:365–373. http://dx.doi.org/10.1083/jcb.93.2.365

Desai, A., P.S. Maddox, T.J. Mitchison, and E.D. Salmon. 1998. Anaphase A chromosome movement and poleward spindle microtubule flux occur at similar rates in *Xenopus* extract spindles. *J. Cell Biol.* 141:703–713. http://dx.doi.org/10.1083/jcb.141.3.703

Dick, A.E., and D.W. Gerlich. 2013. Kinetic framework of spindle assembly checkpoint signalling. *Nat. Cell Biol.* 15:1370–1377. http://dx.doi.org/10.1038/ncb2842

Dionne, M.A., L. Howard, and D.A. Compton. 1999. NuMA is a component of an insoluble matrix at mitotic spindle poles. *Cell Motil. Cytoskeleton*. 42:189–203. http://dx.doi.org/10.1002/(SICI)1097-0169(1999)42:3<189::AID-CM3>3.0.CO;2-X

Ferraro-Gideon, J., R. Sheykhani, Q. Zhu, M.L. Duquette, M.W. Berns, and A. Forer. 2013. Measurements of forces produced by the mitotic spindle using optical tweezers. *Mol. Biol. Cell*. 24:1375–1386. http://dx.doi.org/10.1091/mbc.E12-12-0901

Firestone, A.J., J.S. Weinger, M. Maldonado, K. Barlan, L.D. Langston, M. O'Donnell, V.I. Gelfand, T.M. Kapoor, and J.K. Chen. 2012. Small-molecule inhibitors of the AAA+ ATPase motor cytoplasmic dynein. *Nature*. 484:125–129. http://dx.doi.org/10.1038/nature10936

Gaglio, T., A. Saredi, and D.A. Compton. 1995. NuMA is required for the organization of microtubules into aster-like mitotic arrays. *J. Cell Biol.* 131:693–708. http://dx.doi.org/10.1083/jcb.131.3.693

Gorbsky, G.J., P.J. Sammak, and G.G. Borisy. 1987. Chromosomes move poleward in anaphase along stationary microtubules that coordinately disassemble from their kinetochore ends. *J. Cell Biol.* 104:9–18. http://dx.doi.org/10.1083/jcb.104.1.9

Hayden, J.H., S.S. Bowser, and C.L. Rieder. 1990. Kinetochores capture astral microtubules during chromosome attachment to the mitotic spindle: direct visualization in live newt lung cells. *J. Cell Biol.* 111:1039–1045. http://dx.doi.org/10.1083/jcb.111.3.1039

Holland, A.J., W. Lan, S. Niessen, H. Hoover, and D.W. Cleveland. 2010. Polo-like kinase 4 kinase activity limits centrosome overduplication by autoregulating its own stability. *J. Cell Biol.* 188:191–198. http://dx.doi.org/10.1083/jcb.200911102

Inoué, S., and E.D. Salmon. 1995. Force generation by microtubule assembly/disassembly in mitosis and related movements. *Mol. Biol. Cell*. 6:1619–1640. http://dx.doi.org/10.1091/mbc.6.12.1619

Kapoor, T.M., M.A. Lampson, P. Hergert, L. Cameron, D. Cimini, E.D. Salmon, B.F. McEwen, and A. Khodjakov. 2006. Chromosomes can congress to the metaphase plate before biorientation. *Science*. 311:388–391. http://dx.doi.org/10.1126/science.1122142

Khodjakov, A., R.W. Cole, B.F. McEwen, K.F. Buttle, and C.L. Rieder. 1997a. Chromosome fragments possessing only one kinetochore can congress to the spindle equator. *J. Cell Biol.* 136:229–240. http://dx.doi.org/10.1083/jcb.136.2.229

Khodjakov, A., R.W. Cole, and C.L. Rieder. 1997b. A synergy of technologies: combining laser microsurgery with green fluorescent protein tagging. *Cell Motil. Cytoskeleton*. 38:311–317. http://dx.doi.org/10.1002/(SICI)1097-0169(1997)38:4<311::AID-CM1>3.0.CO;2-6

Khodjakov, A., L. Copenagle, M.B. Gordon, D.A. Compton, and T.M. Kapoor. 2003. Minus-end capture of preformed kinetochore fibers contributes to spindle morphogenesis. *J. Cell Biol.* 160:671–683. http://dx.doi.org/10.1083/jcb.200208143

Kim, Y., J.E. Heuser, C.M. Waterman, and D.W. Cleveland. 2008. CENP-E combines a slow, processive motor and a flexible coiled coil to produce an essential motile kinetochore tether. *J. Cell Biol.* 181:411–419. http://dx.doi.org/10.1083/jcb.200802189

Kleylein-Sohn, J., B. Pöllinger, M. Ohmer, F. Hofmann, E.A. Nigg, B.A. Hemmings, and M. Wartmann. 2012. Acentrosomal spindle organization renders cancer cells dependent on the kinesin HSET. *J. Cell Sci.* 125:5391–5402. http://dx.doi.org/10.1242/jcs.107474

Kukulski, W., M. Schorb, S. Welsch, A. Picco, M. Kaksonen, and J.A. Briggs. 2011. Correlated fluorescence and 3D electron microscopy with high sensitivity and spatial precision. *J. Cell Biol.* 192:111–119. http://dx.doi.org/10.1083/jcb.201009037

LaFountain, J.R. Jr., C.S. Cohan, and R. Oldenbourg. 2011. Functional states of kinetochores revealed by laser microsurgery and fluorescent speckle microscopy. *Mol. Biol. Cell*. 22:4801–4808. http://dx.doi.org/10.1091/mbc.E11-06-0494

LaFountain, J.R. Jr., C.S. Cohan, and R. Oldenbourg. 2012. Pac-man motility of kinetochores unleashed by laser microsurgery. *Mol. Biol. Cell*. 23:3133–3142. http://dx.doi.org/10.1091/mbc.E12-04-0314

Lampson, M.A., and I.M. Cheeseman. 2011. Sensing centromere tension: Aurora B and the regulation of kinetochore function. *Trends Cell Biol.* 21:133–140. http://dx.doi.org/10.1016/j.tcb.2010.10.007

Lancaster, O.M., M. Le Berre, A. Dimitracopoulos, D. Bonazzi, E. Zlotek-Zlotkiewicz, R. Picone, T. Duke, M. Piel, and B. Baum. 2013. Mitotic rounding alters cell geometry to ensure efficient bipolar spindle formation. *Dev. Cell*. 25:270–283. http://dx.doi.org/10.1016/j.devcel.2013.03.014

Le Berre, M., J. Aubertin, and M. Piel. 2012. Fine control of nuclear confinement identifies a threshold deformation leading to lamina rupture and induction of specific genes. *Integr. Biol. (Camb.)*. 4:1406–1414. http://dx.doi.org/10.1039/c2ib20056b

Magidson, V., J. Loncarek, P. Hergert, C.L. Rieder, and A. Khodjakov. 2007. Laser microsurgery in the GFP era: a cell biologist's perspective. *Methods Cell Biol*. 82:239–266. http://dx.doi.org/10.1016/S0091-679X(06)82007-8

Magidson, V., C.B. O'Connell, J. Lončarek, R. Paul, A. Mogilner, and A. Khodjakov. 2011. The spatial arrangement of chromosomes during prometaphase facilitates spindle assembly. *Cell*. 146:555–567. http://dx.doi.org/10.1016/j.cell.2011.07.012

Maiato, H., C.L. Rieder, and A. Khodjakov. 2004. Kinetochore-driven formation of kinetochore fibers contributes to spindle assembly during animal mitosis. *J. Cell Biol.* 167:831–840. http://dx.doi.org/10.1083/jcb.200407090

Maiato, H., A. Khodjakov, and C.L. Rieder. 2005. *Drosophila* CLASP is required for the incorporation of microtubule subunits into fluxing kinetochore fibres. *Nat. Cell Biol.* 7:42–47. http://dx.doi.org/10.1038/ncb1207

McDonald, K.L., E.T. O'Toole, D.N. Mastronarde, and J.R. McIntosh. 1992. Kinetochore microtubules in PTK cells. *J. Cell Biol.* 118:369–383. http://dx.doi.org/10.1083/jcb.118.2.369

McIntosh, J.R., M.I. Molodtsov, and F.I. Ataullakhanov. 2012. Biophysics of mitosis. *Q. Rev. Biophys*. 45:147–207. http://dx.doi.org/10.1017/S0033583512000017

Merdes, A., K. Ramyar, J.D. Vechio, and D.W. Cleveland. 1996. A complex of NuMA and cytoplasmic dynein is essential for mitotic spindle assembly. *Cell*. 87:447–458. http://dx.doi.org/10.1016/S0092-8674(00)81365-3

Micheva, K.D., and S.J. Smith. 2007. Array tomography: a new tool for imaging the molecular architecture and ultrastructure of neural circuits. *Neuron*. 55:25–36. http://dx.doi.org/10.1016/j.neuron.2007.06.014

Nicklas, R.B. 1983. Measurements of the force produced by the mitotic spindle in anaphase. *J. Cell Biol.* 97:542–548. http://dx.doi.org/10.1083/jcb.97.2.542

Nicklas, R.B. 1989. The motor for poleward chromosome movement in anaphase is in or near the kinetochore. *J. Cell Biol.* 109:2245–2255. http://dx.doi.org/10.1083/jcb.109.5.2245

Nicklas, R.B., D.F. Kubai, and T.S. Hays. 1982. Spindle microtubules and their mechanical associations after micromanipulation in anaphase. *J. Cell Biol.* 95:91–104. http://dx.doi.org/10.1083/jcb.95.1.91

O'Haver, T.C. 2009. Peak Fitter, Version 5.4. http://www.mathworks.com/matlabcentral/fileexchange/23611-peak-fitter (accessed June 23, 2014).

Radulescu, A.E., and D.W. Cleveland. 2010. NuMA after 30 years: the matrix revisited. *Trends Cell Biol.* 20:214–222. http://dx.doi.org/10.1016/j.tcb.2010.01.003

Rieder, C.L. 1981. The structure of the cold-stable kinetochore fiber in metaphase PtK1 cells. *Chromosoma*. 84:145–158. http://dx.doi.org/10.1007/BF00293368

Rieder, C.L., and G. Cassels. 1999. Correlative light and electron microscopy of mitotic cells in monolayer cultures. *Methods Cell Biol.* 61:297–315. http://dx.doi.org/10.1016/S0091-679X(08)61987-1

Rieder, C.L., R.W. Cole, A. Khodjakov, and G. Sluder. 1995. The checkpoint delaying anaphase in response to chromosome monoorientation is mediated by an inhibitory signal produced by unattached kinetochores. *J. Cell Biol.* 130:941–948. http://dx.doi.org/10.1083/jcb.130.4.941

Rusan, N.M., U.S. Tulu, C. Fagerstrom, and P. Wadsworth. 2002. Reorganization of the microtubule array in prophase/prometaphase requires cytoplasmic dynein-dependent microtubule transport. *J. Cell Biol.* 158:997–1003. http://dx.doi.org/10.1083/jcb.200204109

Shah, J.V., E. Botvinick, Z. Bonday, F. Furnari, M. Berns, and D.W. Cleveland. 2004. Dynamics of centromere and kinetochore proteins; implications for checkpoint signaling and silencing. *Curr. Biol.* 14:942–952. http://dx.doi.org/10.1016/j.cub.2004.05.046

Sheykhani, R., N. Baker, V. Gomez-Godinez, L.H. Liaw, J. Shah, M.W. Berns, and A. Forer. 2013. The role of actin and myosin in PtK2 spindle length changes induced by laser microbeam irradiations across the spindle. *Cytoskeleton (Hoboken)*. 70:241–259. http://dx.doi.org/10.1002/cm.21104

Spurck, T.P., O.G. Stonington, J.A. Snyder, J.D. Pickett-Heaps, A. Bajer, and J. Mole-Bajer. 1990. UV microbeam irradiations of the mitotic spindle. II. Spindle fiber dynamics and force production. *J. Cell Biol.* 111:1505–1518. http://dx.doi.org/10.1083/jcb.111.4.1505

Tanaka, K., N. Mukae, H. Dewar, M. van Breugel, E.K. James, A.R. Prescott, C. Antony, and T.U. Tanaka. 2005. Molecular mechanisms of kinetochore capture by spindle microtubules. *Nature*. 434:987–994. http://dx.doi.org/10.1038/nature03483

Tulu, U.S., N.M. Rusan, and P. Wadsworth. 2003. Peripheral, non-centrosome-associated microtubules contribute to spindle formation in centrosome-containing cells. *Curr. Biol.* 13:1894–1899. http://dx.doi.org/10.1016/j.cub.2003.10.002

Tulu, U.S., C. Fagerstrom, N.P. Ferenz, and P. Wadsworth. 2006. Molecular requirements for kinetochore-associated microtubule formation in mammalian cells. *Curr. Biol.* 16:536–541. http://dx.doi.org/10.1016/j.cub.2006.01.060

Walczak, C.E., S. Cai, and A. Khodjakov. 2010. Mechanisms of chromosome behaviour during mitosis. *Nat. Rev. Mol. Cell Biol.* 11:91–102. http://dx.doi.org/10.1038/nrm2832

Witt, P.L., H. Ris, and G.G. Borisy. 1981. Structure of kinetochore fibers: microtubule continuity and inter-microtubule bridges. *Chromosoma*. 83:523–540. http://dx.doi.org/10.1007/BF00328277

Yang, Z., U.S. Tulu, P. Wadsworth, and C.L. Rieder. 2007. Kinetochore dynein is required for chromosome motion and congression independent of the spindle checkpoint. *Curr. Biol.* 17:973–980. http://dx.doi.org/10.1016/j.cub.2007.04.056